J Mater Sci (2016) 51:344–352
DOI 10.1007/s10853-015-9347-8

50TH ANNIVERSARY

Interfacial and internal stress transfer in carbon nanotube based nanocomposites

Robert J. Young[1] · Libo Deng[1,2] · Tamer Z. Wafy[1,3] · Ian A. Kinloch[1]

Received: 29 May 2015 / Accepted: 7 August 2015 / Published online: 18 August 2015

Abstract This study is concerned with structure–property relationships in different types of carbon nanotubes (CNTs), in particular investigating both interfacial and internal stress transfer for CNTs in nanocomposites. The shift of position and width of the G′-Raman band for single-walled CNTs (SWNTs) and multi-walled CNTs (MWNTs) in an epoxy matrix were used to monitor stress transfer between the nanotubes and an epoxy matrix in nanocomposites. It was found that the rate of band shift per unit strain was higher for the SWNTs than the MWNTs and that the G′ band tended to undergo broadening with strain for the SWNTs and narrowing with strain for the MWNTs. A theory has been developed to simulate this behaviour in terms of stress transfer between the different layers within the MWNTs. It has also enabled the determination of the stress transfer efficiency parameter, (k_i) for the MWNTs. It is demonstrated that MWNTs give inferior reinforcement to SWNTs as a result of slippage between the walls giving rise to poor internal stress transfer in the MWNTs. This phenomenon will lead to the MWNTs having a lower effective Young's modulus in nanocomposites than SWNTs.

Electronic supplementary material The online version of this article (doi:10.1007/s10853-015-9347-8) contains supplementary material, which is available to authorized users.

✉ Robert J. Young
robert.young@manchester.ac.uk

[1] School of Materials, University of Manchester, Manchester M13 9PL, UK

[2] Shenzhen Institute of Advanced Technology, Chinese Academy of Sciences, Shenzhen 518055, China

[3] Military Technical College, Kobry Elkobbah, Cairo, Egypt

Introduction

Carbon nanotubes (CNTs) are long cylinders of sp^2 hybridized covalently bonded carbon atoms. There are basically two main types of CNTs depending upon the number of graphene cylinders in their structure as shown in Fig. 1: single-wall nanotubes (SWNTs) and multi-wall nanotubes (MWNTs); double-wall nanotubes (DWNTs) are a special case of MWNTs. CNTs possess extremely high values of Young's modulus (~1 TPa) and strength (~120 GPa), and these mechanical properties have prompted many scientists to consider them as reinforcements in composite materials [1, 2].

The surface and interface play an important role in controlling the properties of a broad range of composite materials including CNT/epoxy nanocomposites [2]. The development of improved high-performance polymer nanocomposites based on CNTs can only be achieved by simultaneously optimizing the CNT aspect ratio, dispersion, packing, bonding between the epoxy and CNTs at the interface, inter-wall sliding within CNTs under tension, and reduced polymer shrinkage during processing. Raman spectroscopy can be used to characterize the deformation behaviour of CNTs in composites [3]. Evidence of stress transfer between the matrix and the CNTs can be observed from the stress-induced shifts of the Raman bands.

Recently, researchers have shown interest in following stress transfer from the positions of the stress-sensitive G′ (or 2D), G and D bands as well as the intensities of the radial breathing modes (RBM) bands [4, 5] to follow the deformation of SWNT bundles (and detect interface damage) [6], DWNTs [7], MWNTs in epoxy nanocomposites [3], and CNT fibres [8]. Applying external strains that modify the electronic structure of CNTs in epoxy nanocomposites causes shifts in their Raman peak positions

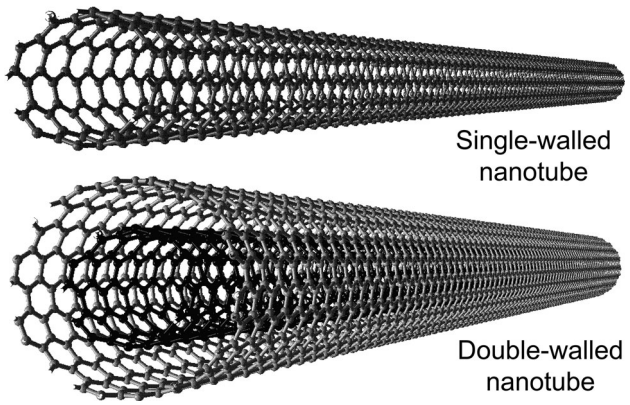

Fig. 1 Schematic representations of single- and double-walled carbon nanotubes. Multi-walled nanotubes can have more than 100 layers of nested tubes. (Courtesy of Dr. F. Ding, Hong Kong Polytechnic University.)

(G, D and G′) as well as the linewidths and the intensities of the RBMs. Far less attention has been paid, however, to the corresponding band width changes, in particular the changes in full-width half maximum (FWHM) in the Raman peaks, from which other important information can be obtained.

The aim of this study was to determine and evaluate the interfacial interactions of nanotubes with epoxy polymers detected from G′-frequency shifts and the corresponding changes in the FWHM. The Raman response of SWNTs and MWNTs in epoxy nanocomposites during tensile deformation process has been simulated, and the results of the simulations are compared with the experimental observations. The similarities and differences between the predicted and observed behaviour of SWNTs and MWNTs in epoxy nanocomposites have been investigated in detail and the behaviour interpreted in terms of interfacial and internal stress transfer in the two types of nanotubes.

Materials and methods

Carbon nanotubes

The SWNTs (HiPco material) were used as-received from Carbon Nanotechnologies, Inc., of Houston, USA. The MWNTs used in this study were synthesized using a chemical vapour deposition (CVD) process adapted from Singh et al. [9]. A solution of 5 wt% ferrocene in toluene was injected at a rate of 0.04 ml/min into an argon gas stream pre-heated to 200 °C and flowing at 100 ml/min. The reactants were carried into the reaction zone which was at 760 °C, where the nanotubes were grown on a quartz surface. The reaction time was 4 h, after which the reactor was cooled to room temperature under argon and the MWNTs harvested from the growth substrates.

The microstructures of SWNTs and MWNTs were characterized by transmission electron microscopy (TEM) using a Philips CM200 TEM with a tungsten filament operated at 200 kV.

Nanocomposite preparation

The matrix system used in this study was a low viscosity epoxy resin supplied by Huntsman Co. It consists of Araldite LY5052 as an epoxy phenol novolak resin and Aradur 5052 CH as a liquid polyamine hardener with a weight mixing ratio of 100:38, respectively. The MWNTs were used as-made and the SWNTs as-received.

An extensive mixing procedure was used to ensure good dispersion of the CNTs. They were suspended in ethanol (17 g) using an ultrasonic bath for 1.5 h. The resin (100 g) was then added to the mixture, which was sonicated for a further 4 h. For homogenization, the mixture was stirred at room temperature using a mechanical stirrer for two days, followed by sonication in the bath for 8 h. In order to remove ethanol residues, the mixture was stirred mechanically (100 rpm, 85 °C) and then at 50 °C for 7 and 12 h, respectively. For de-gassing, the mixture was left in a thermostatted vacuum oven (at 70 °C for 30 min). The hardener was added, after the mixture was cooled to room temperature, and stirred mechanically for 10 min. The mixture was put into a vacuum oven to de-gas for a further 15 min. For Raman analysis, samples were prepared by carefully casting the mixture into a stainless steel square mould (160 × 160 × 3 mm).

The nanocomposites were then cured at 100 °C for 2 h, removed immediately from the oven and left to cool at room temperature. For Raman investigations and thermo-mechanical measurements, the nanocomposite samples were cut into rectangular specimens. The nanocomposite samples were prepared for comparative purposes, with concentrations of SWNTs and MWNTs of 0.1 wt%.

Raman spectroscopy and in situ deformation

The Raman spectra of the nanocarbon powders and nanocarbon/epoxy nanocomposites were obtained at room temperature using a Renishaw Raman imaging microscope system 1000 with an Olympus BHM microscope. A notch (Rayleigh line rejection) filter with a limit of 100 cm^{-1} was used. An excitation frequency of 633 nm (1.96 eV) polarized laser beam, and a back-scattering geometry was used to collect the Raman signals without the use of a polarization analyser.

A fixed laser power was employed with maximum value of 1.20 mW and focused to a spot size of about 1 μm in diameter with an MD plan ×50 objective lens (numerical

aperture 0.75). Spectra were acquired in the range 2500–2800 cm^{-1} and over 100–3000 cm^{-1} (Stokes shift) with the continuous extended grating mode. The spectra collection was repeated a number of times to reduce the signal noise. All the Raman band spectra were analysed by Lorentzian routines. For the same batch of material, the Raman spectra are presented as the average of spectra from three different specimens.

For deformation, the rectangular specimens with dimensions of 61-mm length, 14-mm width, and 3-mm thickness were loaded stepwise using a four-point bending rig, which was located on the Raman microscope stage. The Raman spectra were obtained with the laser beam focused on the tensile surface of the beam. The composite beams were deformed step-by-step in ~0.1 % strain intervals, determined from strain gauges, with a gauge factor of 2.09 attached to the tensile surface by cyanoacrylate adhesive. The conditions for tensile deformation of CNT/epoxy nanocomposites were loading of the nanocomposites up to 1.5 % strain with several Raman spectra obtained at each strain level. The Raman spectra were determined as a function of the strain recorded on the strain gauge after any relaxation had occurred.

Results

The morphology of the CNTs

Figure 2 shows TEM images of the SWNTs and MWNTs. In general, most of the HiPco SWNTs consist of bundles, 40 ± 25 nm in size, consisting of well-aligned nanotubes as shown by TEM and accompanied by numerous residual iron catalyst particles of around 3–4 nm in diameter. The diameters of the SWNTs, deduced from the Raman wavenumber of the RBM modes [10], were mostly in the range 0.6–1.7 nm and with an average diameter of 1.02 ± 0.22 nm.

The morphology of the MWNTs was first observed by scanning electron microscopy which showed bundles of entangled tubes, 225 ± 85 μm in length. Most of the MWNTs have irregular curved and entangled tubular structures that are hollow inside. They were shown by TEM to have 61 ± 24 and 9 ± 3 nm outer and inner diameters, respectively, accompanied by numerous iron particles around 72 ± 37 nm in length and 13 ± 5 nm in diameter. Some encapsulated particles and other particles attached to the nanotube walls were observed for the MWNTs. Lattice

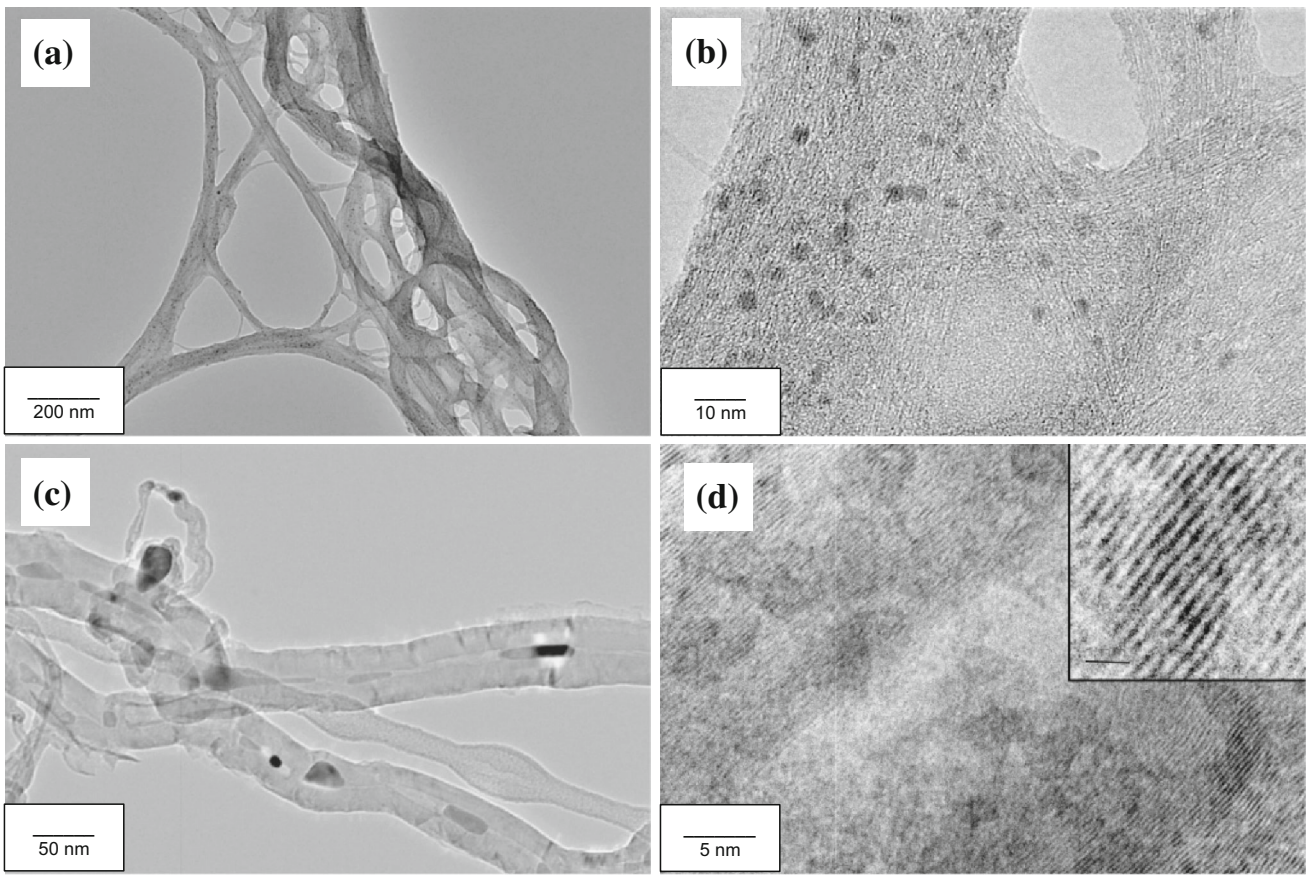

Fig. 2 TEM images of the CNT powders at different magnifications with *scale bars* for as-received SWNTs **a** 200 nm, **b** 10 nm, and for as-grown MWNTs **c** 50 nm, **d** 5 nm with an inset image of the inner layers of single MWNT nanotube

fringes from the graphene layers with a 0.33 nm spacing can be seen in the inset in the TEM image in Fig. 2d.

Raman spectra of CNTs in epoxy nanocomposites

Figure 3 shows the Raman spectra of the hot-cured epoxy resin, the SWNTs, and MWNTs, and their epoxy composites excited using a 633 nm (He–Ne) laser. The high relative intensities of the Raman bands of all the CNTs, even at 0.1 wt% loading, compared to the epoxy bands in the nanocomposites are due to the strong resonance Raman scattering from the CNTs [10].

Figures 3b, d compare the G′-bands of the SWNTs and MWNTs either in the powder form or in their epoxy composites in the range 2500–2800 cm^{-1}. The G′-bands of SWNTs and MWNTs are still well-defined but their frequency is upshifted by about 10 cm^{-1} in the composites. This may be the result of the generation of internal residual compressive stresses induced during the curing shrinkage, as well as thermal shrinkage during cooling from the cure temperature [11].

Effect of deformation upon the Raman spectra of CNT/epoxy nanocomposites

Figure 4a shows the shift of G′-band frequencies of the SWNTs and MWNTs in the epoxy composites during tensile deformation up to 1.5 % strain and it can be seen that there is a general downshift of the G′-band. The initial shift rate was found to be -14.1 ± 3.3 cm^{-1}/% strain for the SWNTs compared with a much lower value of −3.4 ± 1.3 cm^{-1}/% strain for the MWNTs in the same resin cured under the same conditions. It should be noted that the difference in initial band positions between the MWNTs and SWNTs is due in part to the difference in their diameters (see Fig. 2) [10].

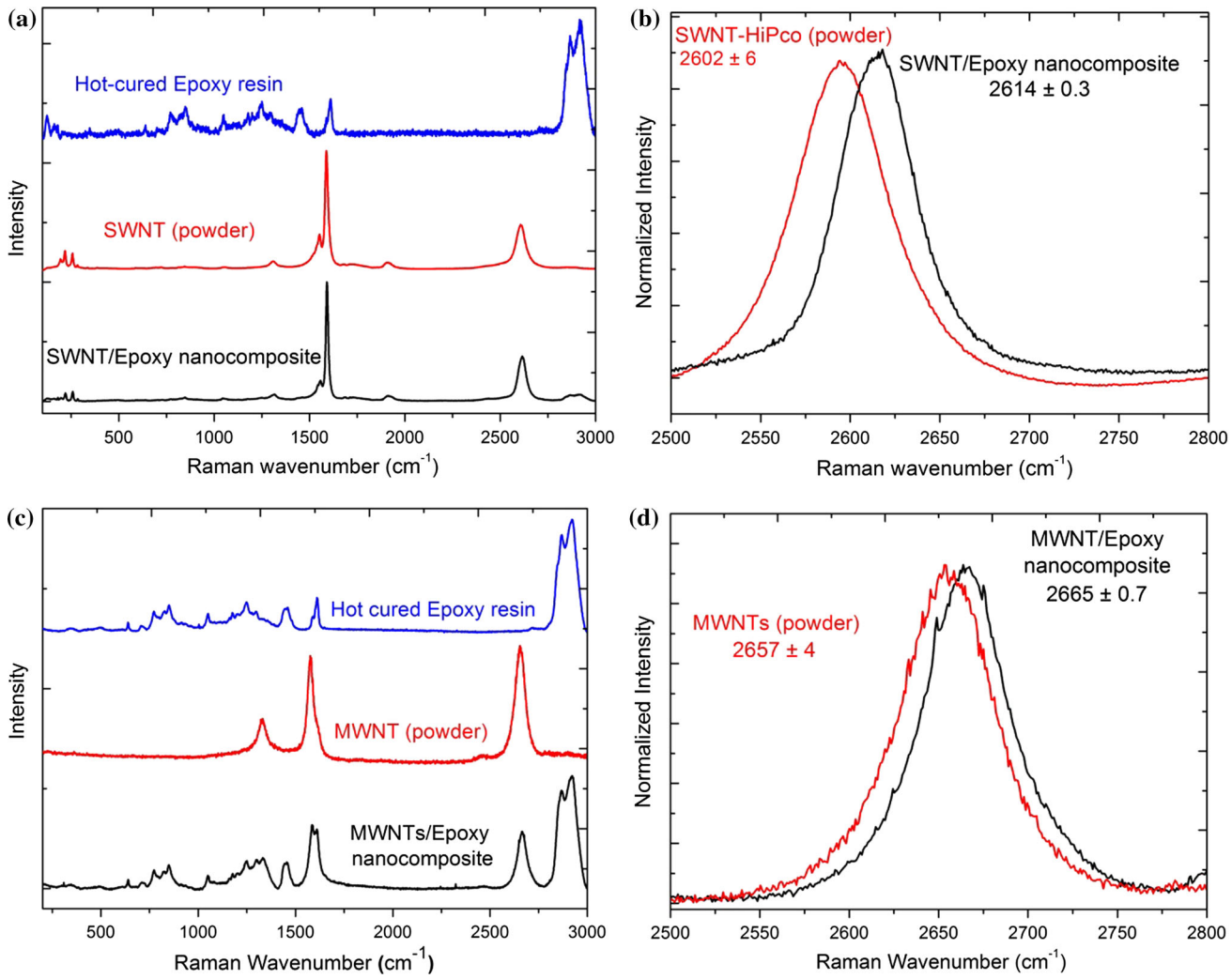

Fig. 3 **a**, **c** Raman spectra of the epoxy resin, the SWNTs, and MWNTs, respectively, and hot-cured CNT/epoxy nanocomposites in the range 1000–3000 cm^{-1} excited using 633 nm (He–Ne) laser. **b**, **d** G′-Raman spectra of SWNT and MWNT powder and hot-cured SWNT/epoxy nanocomposites in the range 2500–2800 cm^{-1}

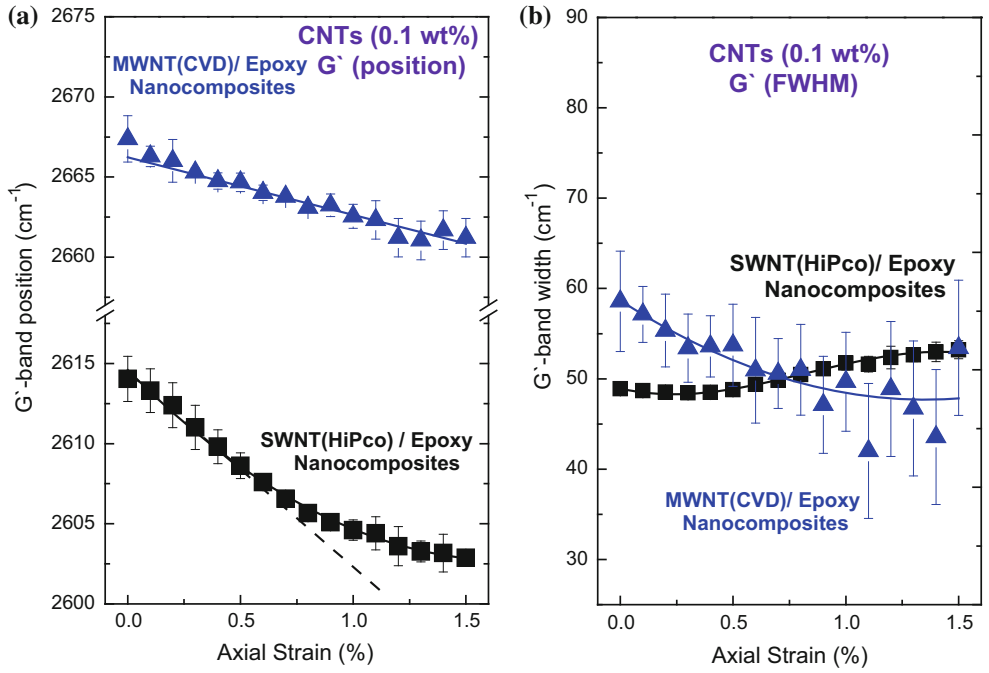

Fig. 4 **a** The shift of the G′-band positions and **b** the change of widths of the G′-band (FWHM) for hot-cured SWNT and MWNT/epoxy composites up to 1.5 % maximum loading strain fitted to one Lorentzian peak

Figure 4b shows the G′ band widths (full width at half maximum, FWHM) plotted as a function of strain for the two CNT/epoxy composites. There is a striking difference between the two CNT materials in that the G′ band width of the SWNTs increases (broadening) while that of the MWNTs decreases (narrowing) with tensile strain. It should be noted that there is rather more scatter in the band width data for the MWNTs because the intensity of their G′ band is less than that of the SWNTs (Fig. 3) leading more error in the curve fitting procedure. There are similarities between the broadening behaviour of the G′ band widths in this study and the G band widths described by Kumar et al. [12]. The authors assumed that the strain-induced broadening observed in their semiconducting SWNTs was a result of inhomogeneous deformation, which is expected if the strain is not uniformly distributed between the nanotubes. This would not, however, explain the anomalous band narrowing behaviour of the MWNTs. This is the subject of this present study.

It has been established that the G′-band shift rate is related to the effective Young's modulus, E_{eff}, of the CNTs in a composite [13]. The initial shift rate of $S(0) = -14.1 \pm 3.3$ cm^{-1}/% strain for the SWNTs is over four times higher than $S(0)$ for the MWNTs at the same loading of nanotubes (0.1 wt%) in the same epoxy resin prepared in an identical way. This implies that the E_{eff} of the SWNTs is over four times higher than that of the MWNTs [12]. Consideration will now be given to why this is the case.

Discussion

SWNT/epoxy nanocomposites

Considerable work has been undertaken using Raman spectroscopy to investigate the deformation of SWNTs in SWNT/polymer composites to probe degradation of the interface between the polymers and nanotubes [14], to measure the interfacial shear strength of the SWNT–matrix interface [6] and to map the strain fields around fibres in a glass fibre–reinforced polymer composite [15, 16]. This has been undertaken by following the deformation of the nanotubes using the shifts of the D-, G-, G′- Raman band frequencies. The G′-Raman band has the highest shift rate per unit strain which for individual isolated SWNTs can be as large as -40 cm^{-1}/% strain [17] which approaches the value of the 2D (or G′) band shift rate of -60 cm^{-1}/% strain for graphene [18]. In the nanocomposites, $S(0)$ is significantly lower and ranges from -1.3 to -15 cm^{-1}/% strain. This wide range has been attributed to the SWNT bundle size, dispersion of the nanotubes, variations in nanotube orientation, as well as differences in interfacial adhesion to the matrix [19]. Our value of band shift rate, at the top of this range, implies that in our nanocomposites there is a reasonable dispersion of SWNTs with strong interfacial adhesion to the matrix.

It has been demonstrated that the frequency of the G′-peak depends on the tube diameter of the isolated SWNTs [10] through

$$\omega_{G'} = \omega_{G'_0} - \left(\frac{35.4}{D}\right), \quad (1)$$

where $\omega_{G'_0}$ is the frequency G′-band in graphene (cm^{-1}) that is laser energy dependent and D is the diameter (nm) of the individual tubes in the MWNTs and SWNTs. The SWNT powder has a value of $\omega_{G'}$ of 2602 ± 6 cm^{-1} which yields a value for monolayer graphene at the laser wavelength used of $\omega_{G'_0} = 2637 \pm 6$ cm^{-1}, which is close to the accepted value for graphene [10].

The G′ band shift rate $S(0)$ is defined as

$$S(0) = d\omega_{G'}/d\varepsilon, \quad (2)$$

where ε is the strain in the nanocomposite. Hence at a given strain ε, the value frequency of the Raman G′ band will be

$$\omega_{G'_{CNT}} = \omega_{G'_0} + S(0)\varepsilon - \left(\frac{35.4}{D}\right) \quad (3)$$

for a SWNT of diameter D. The dashed line in Fig. 4a corresponds to this equation plotted for the SWNT nanocomposite with $S(0) = -14.1$ $cm^{-1}/\%$ strain. It should be noted that the value of $\omega_{G'_{CNT}}$ at zero strain in this case is 2614 ± 2 cm^{-1} rather than the 2602 ± 6 cm^{-1} found for the SWNT powder. This is the result of the SWNTs being subjected to compression as a result of resin shrinkage during curing. This is assumed to not affect the value of $S(0)$.

It can be seen in Fig. 4a that the experimental data deviate from the dashed line above around 0.5 % strain due probably to slippage at the SWNT–matrix interface [8], behaviour not found for the MWNTs. The TEM images in Fig. 2 show marked differences between the morphology of the two types of nanotubes. The MWNTS have an irregular cross-section that may help to anchor the MWNT/epoxy interface during deformation. The SWNTs are smooth and bundled so that SWNT/SWNT and/or SWNT/epoxy interfacial slippage may be easier during deformation. It should also be noted that Fig. 4b shows that the G′ band for the SWNTs undergoes broadening above around 0.5 % strain which is similar to the behaviour of graphene monolayers for which the G′(2D) band undergoes broadening with strain [10] but there could again be contributions from slippage and local strain differences in the SWNTs in the nanocomposites.

MWNT/epoxy nanocomposites

In view of the lower G′ Raman band shift rate for the MWNTs, an exercise has been undertaken to model their deformation in nanocomposites. This is shown in detail in the Supplementary Material and only a brief outline will be given here.

It is assumed in the model that the SWNTs and MWNTs have an identical dispersion, and stress transfer at the nanotube–matrix interface is the same at low strains. It is assumed further that the only difference is that in the MWNTs stress transfer to the inner walls has to take place by shear between the different graphene layers. The model chosen is shown schematically in Fig. 5 and is based upon that employed earlier for DWNTs [7]. The nanotubes can be characterized in terms of their chiral vectors. The SWNTs ($n = 1$) are described by a (5, 5) layer and the family of ten coaxial commensurate tubes for MWNTs which it can be presented by $(5n, 5n)$, $(5n - 1, 5n - 1)$, $(5n - 2, 5n - 2)$,…, $(5n - 9, 5n - 9)$ for the outermost wall, the ninth wall, the eighth wall,…, and the innermost wall, respectively. The separation between individual walls in MWNTs is constant (~ 0.35 nm) for this family in tubes. The outermost wall $(5n, 5n)$ is in contact directly with the epoxy polymer matrix. The relationship between the transmittance of light T % and the number of graphene layers has been widely investigated, and monolayer graphene is found to transmit about 97.7 % of visible white

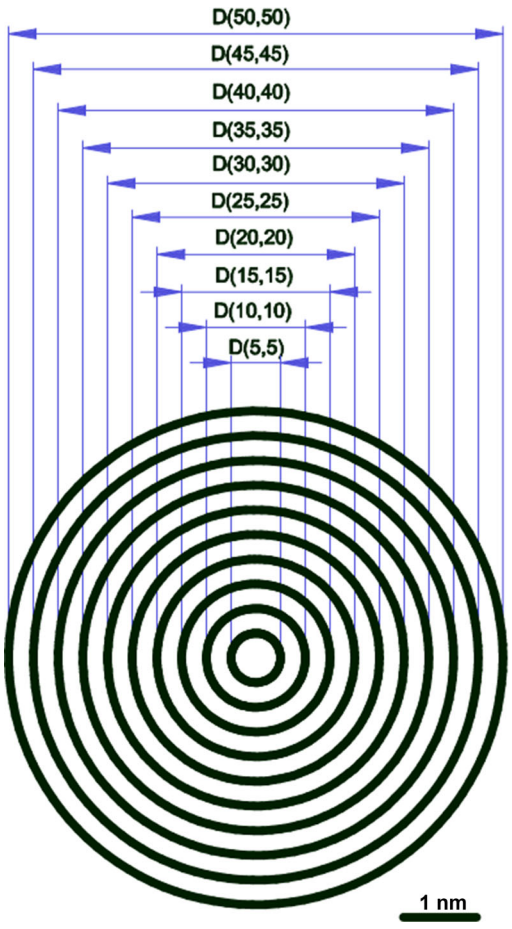

Fig. 5 The geometry for model of the MWNTs where $n = 10$. The outermost wall (50, 50) is in contact directly with the polymer epoxy matrix

light [20]. This factor has also been taken into account in the model for the MWNTs (see Supplementary Material).

Through this stress transfer model for MWNTs, the Raman spectra of the stress-induced shift rate of the G′-band in CNTs in epoxy composites have been simulated to estimate the load transfer efficiency of any nanotubes in the ($5n$, $5n$) family where n is an integer. The G′-band was chosen because it has a higher strain sensitivity compared with the Raman first-order bands, particularly at low levels of strain.

If there is perfect stress transfer between the individual layers in the MWNTs then it would be expected that during deformation there would be the same band shift rate, $S(0)$, between each layer. If the stress transfer is not perfect, the stress transfer efficiency can be described by a factor k_i ($0 \leq k_i \leq 1$) [7, 21]. In the case of no stress transfer, $k_i = 0$, and in the case of perfect stress transfer, $k_i = 1$. For the MWNTs in which the internal stress transfer is not perfect, it would be expected that $S(0)$ would be reduced by a factor of k_i for each successive layer such that that measured band shift rate for the MWNTs would be lower than that for the equivalent SWNTs. The analysis outlined below (and in the Supplementary Material) explains how this may be modelled.

The individual components of the G′-band from the family of the nanotubes and the resultant overall G′ band are presented in Fig. 6. In order to know the appropriate value of the stress transfer efficiency parameters, k_i, for the experimental shift of the Raman G′ bands, the value of the stress transfer efficiency parameters, k_i, was varied between zero and one in steps of 0.1 as shown in Fig. 7.

The calculations of the resulting line shapes of the G′-peak-induced stresses, for 10 layers, yield a best fit with a shear transfer efficiency parameter, $k_i \approx 0.7$. The shear transfer efficiency parameters corresponding to perfect and no shear transfer (full slip) are $k_i = 1.0$ and $k_i = 0$ [7, 21], respectively, as shown in Fig. 7. The reason for a shear transfer efficiency parameter of $k_i \approx 0.7$ could be attributed to the imperfect interface bonding between layers, and therefore, the shear stress decreases steadily as the number of layers increases. Consequently, the load is taken mainly by the outside layer, and the inner layers offer decreasing reinforcement. A previous study of DWNTs produced by the pea-pod route [7] showed that there was very poor internal stress transfer in these materials ($k_i \approx 0.1$). A value of $k_i \approx 0.7$ for the MWNTs in this present study made by a CVD process indicates rather better internal stress transfer for these CVD-produced MWNT materials.

Comparisons between the experimental and simulated of the G′-bands downshifts for the MWNTs are presented in Fig. 8a. It is observed that the G′ band shifts approximately linearly which suggests that there is good bonding between the MWNTs and epoxy matrix. However, on increasing the

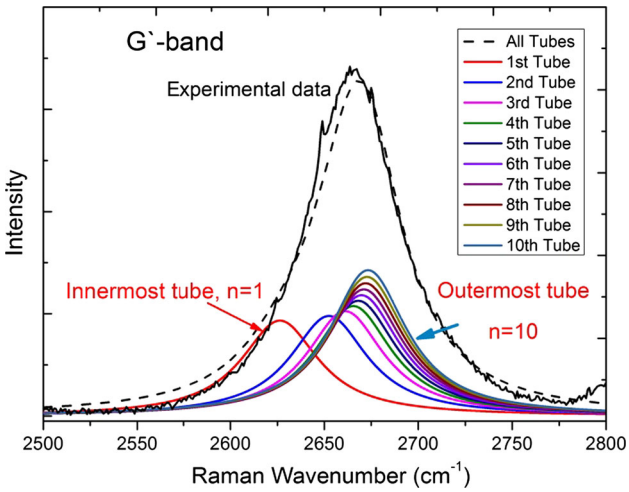

Fig. 6 The simulated Raman spectrum for G′ bands for MWNTs in MWNT/epoxy nanocomposites at 0 % strain

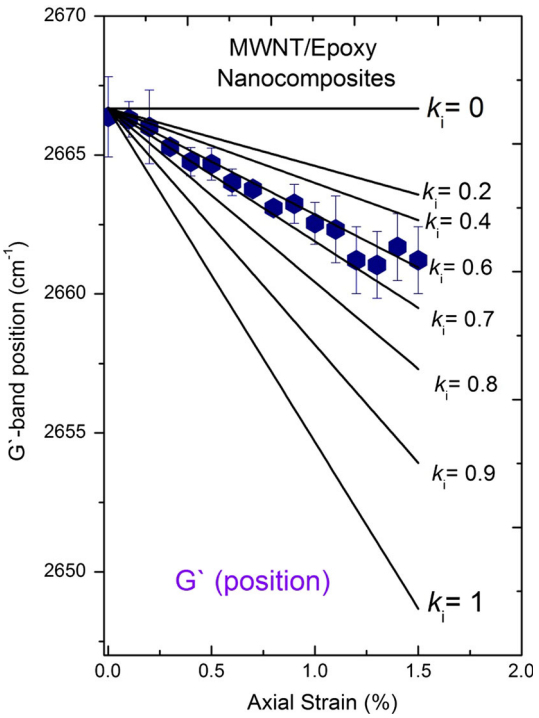

Fig. 7 The experimental shift of the Raman G′ bands positions (solid hexagons) and their corresponding model simulation as a function of strain from 0 to 1.5 % for hot-cured 0.1 wt% MWNT/epoxy nanocomposites and the different values of the stress transfer efficiency parameters, k_i as a function of strain from 0 to 1.5 %

tensile strain, the shift becomes slightly non-linear indicating some minor interfacial slippage. The most striking result to emerge from Fig. 8b for MWNTs/epoxy composites is that there is narrowing of the G′-band up to 1.5 % strain in both the experimental and simulated data, not found for the SWNTs. This behaviour is most likely due to imperfect internal stress transfer leading to the outer walls

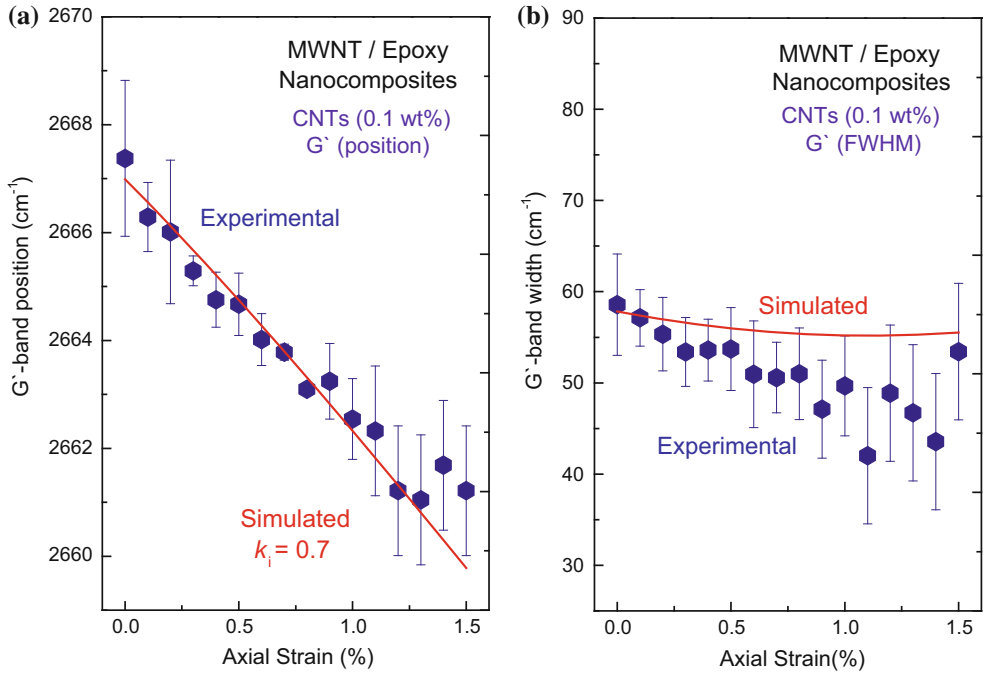

Fig. 8 **a** Experimental shift of the Raman G′ bands positions and their corresponding model simulation and **b** experimental shift of the Raman G′ bands widths (FWHM) and their corresponding model simulation as a function of strain from 0 to 1.5 % for the hot-cured 0.1 wt% MWNT/epoxy nanocomposite, where $k_i \approx 0.7$ for the simulated data

in the MWNTs becoming more highly strained than the inner walls, leading to larger band shifts for the outer wall higher wavenumber components of the G′ band spectrum causing band narrowing (Fig. 6). Even though there is not exact agreement between the experimental and simulated data, it is clear that the modelling captures the essence of the behaviour.

Conclusions

This study has investigated the importance of using Raman spectroscopy to follow stress transfer in epoxy nanocomposites reinforced with CNTs (SWNTs and MWNTs) to enable the reinforcing ability of the CNTs in an epoxy matrix to be elucidated. In particular, the study was undertaken to assess the efficiency of stress transfer at the CNT/epoxy interface and between the inner walls of the MWNTs during tensile deformation. Optimized conditions were used to synthesize a high yield of MWNTs, with a high aspect ratio and a well-defined G′ Raman peak that enabled the deformation of the MWNTs to be followed in detail. The most important finding to be drawn is that stress transfer takes place between both types of nanotubes and the polymer matrix, indicating that the reinforcement of the epoxy resin with the different CNTs takes place. Although the examples given are only for SWNTs and MWNTs, it is possible to undertake similar studies for DWNTs [7]. It should also be of interest to analyse the stress transfer behaviour of single chirality nanotubes that are now becoming available [22, 23].

The stress-induced Raman shifts in the nanocomposites have been shown to be controlled by the number of carbon layers in the nanotubes. A theory has been developed to simulate this behaviour and determine the efficiency of stress transfer between the different layers in terms of stress transfer efficiency factor, (k_i), for MWNTs. Overall the best stress transfer and so highest effective Young's modulus are found for the SWNTs, but they were found to undergo interfacial slippage above around 0.5 % strain. The MWNTs have a lower effective Young's modulus as a result of slippage between the internal layers of the CNTs but they appear to show better interfacial stress transfer with the matrix than the SWNTs.

Compliance with ethical standards

Conflict of interest The authors declare that they have no conflict of interest.

References

1. Chou TW, Gao LM, Thostenson ET, Zhang ZG, Byun JH (2010) An assessment of the science and technology of carbon nanotube-based fibers and composites. Comp Sci Technol 70(1):1–19

2. Thostenson ET, Ren ZF, Chou TW (2001) Advances in the science and technology of carbon nanotubes and their composites: a review. Comp Sci Technol 61(13):1899–1912
3. Cooper CA, Young RJ, Halsall M (2001) Investigation into the deformation of carbon nanotubes and their composites through the use of Raman spectroscopy. Compos A Appl Sci Manuf 32(3–4):401–411
4. Lucas M, Young RJ (2004) Effect of uniaxial strain deformation upon the Raman radial breathing modes of single-wall carbon nanotubes in composites. Phys Rev B 69(8):085405
5. Lucas M, Young RJ (2007) Unique identification of single-walled carbon nanotubes in composites. Comp Sci Technol 67(10): 2135–2149
6. Kao CC, Young RJ (2010) Assessment of interface damage during the deformation of carbon nanotube composites. J Mater Sci 45(6):1425–1431. doi:10.1007/s10853-009-3947-0
7. Cui S, Kinloch IA, Young RJ, Noe L, Monthioux M (2009) The effect of stress transfer within double-walled carbon nanotubes upon their ability to reinforce composites. Adv Mater 21(35):3591–3595
8. Vilatela JJ, Deng L, Kinloch IA, Young RJ, Windle AH (2011) Structure of and stress transfer in fibres spun from carbon nanotubes produced by chemical vapour deposition. Carbon 49(13):4149–4158
9. Singh C, Shaffer MS, Windle AH (2003) Production of controlled architectures of aligned carbon nanotubes by an injection chemical vapour deposition method. Carbon 41(2):359–368
10. Saito R, Hofmann M, Dresselhaus G, Jorio A, Dresselhaus MS (2011) Raman spectroscopy of graphene and carbon nanotubes. Adv Phys 60(3):413–550
11. Kao CC, Young RJ (2004) A Raman spectroscopic investigation of heating effects and the deformation behaviour of epoxy/SWNT composites. Comp Sci Technol 64(15):2291–2295
12. Kumar R, Cronin SB (2007) Raman scattering of carbon nanotube bundles under axial strain and strain-induced debundling. Phys Rev B 75(15):155421
13. Deng LB, Eichhorn SJ, Kao CC, Young RJ (2011) The effective Young's modulus of carbon nanotubes in composites. ACS Appl Mater Interfaces 3(2):433–440
14. Deng LB, Young RJ, van der Zwaag S, Picken S (2010) Characterization of the adhesion of single-walled carbon nanotubes in poly (p-phenylene terephthalamide) composite fibres. Polymer 51(9):2033–2039
15. Sureeptanapas P, Young RJ (2009) SWNT composite coatings as a strain sensor on glass fibres in model epoxy composites. Comp Sci Technol 69(10):1547–1552
16. Sureeyatanapas P, Hejda M, Eichhorn SJ, Young RJ (2010) Comparing single-walled carbon nanotubes and samarium oxide as strain sensors for model glass-fibre/epoxy composites. Comp Sci Technol 70(1):88–93
17. Kannan P, Eichhorn SJ, Young RJ (2007) Deformation of isolated single-wall carbon nanotubes in electrospun polymer nanofibres. Nanotechnology 18(23):235707
18. Gong L, Kinloch IA, Young RJ, Riaz I, Jalil R, Novoselov KS (2010) Interfacial stress transfer in a graphene monolayer nanocomposite. Adv Mater 22(24):2694–2697
19. Young K, Blighe FM, Vilatela JJ, Windle AH, Kinloch IA, Deng LB, Young RJ, Coleman JN (2010) Strong dependence of mechanical properties on fiber diameter for polymer-nanotube composite fibers: differentiating defect from orientation effects. ACS Nano 4(11):6989–6997
20. Nair RR, Blake P, Grigorenko AN, Novoselov KS, Booth TJ, Stauber T, Peres NMR, Geim AK (2008) Fine structure constant defines visual transparency of graphene. Science 320(5881):1308
21. Zalamea L, Kim H, Pipes RB (2007) Stress transfer in multi-walled carbon nanotubes. Comp Sci Technol 67(15–16):3425–3433
22. Sanchez-Valencia JR, Dienel T, Groning O, Shorubalko I, Mueller A, Jansen M, Amsharov K, Ruffieux P, Fasel R (2014) Controlled synthesis of single-chirality carbon nanotubes. Nature 512(7512):61–64
23. Yang F, Wang X, Zhang DQ, Yang J, Luo D, Xu ZW, Wei JK, Wang JQ, Xu Z, Peng F, Li XM, Li RM, Li YL, Li MH, Bai XD, Ding F, Li Y (2014) Chirality-specific growth of single-walled carbon nanotubes on solid alloy catalysts. Nature 510(7506):522–524